energy&fuels

Article

Cite This: Energy Fuels 2018, 32, 5799−5811

pubs.acs.org/EF

Experimental Investigation on the Mechanical Behavior of Victorian Brown Coal under Brine Saturation

K. H. S. M. Sampath,[†] M. S. A. Perera,*[,†] D. Elsworth,[‡] P. G. Ranjith,[§] S. K. Matthai,[†] and T. Rathnaweera[§]

[†]Department of Infrastructure Engineering, Engineering Block B, Grattan Street, Parkville, The University of Melbourne, Melbourne, Victoria 3010, Australia

[‡]Energy and Mineral Engineering, G3 Center and EMS Energy Institute, Pennsylvania State University, University Park, Pennsylvania 16801, United States

[§]Department of Civil Engineering, Monash University, Clayton Campus, Clayton, Victoria 3800, Australia

Downloaded via PENNSYLVANIA STATE UNIV on June 20, 2025 at 11:52:09 (UTC).
See https://pubs.acs.org/sharingguidelines for options on how to legitimately share published articles.

ABSTRACT: Successful hydraulic fracturing depends on the characteristics of the induced fracture network, which controls the enhancement of permeability and ultimate gas production. Among the various factors, the brine concentration in the pore fluid can significantly affect the process, through alterations in microstructure and the impacts of this on rock mechanical behavior. This paper investigates the mechanical behavior of coal in terms of UCS, brittleness, and volumetric-strain deformation and characterizes the induced fracture network caused by monocyclic uniaxial compression on coal samples saturated with varying brine concentration (i.e., 0%, 10%, and 20% NaCl by weight). The mechanical analysis suggests that the softening effect due to water saturation and the chemical interactions between ions in the solution and rock mass cause a significant strength reduction. At a higher order of NaCl concentrations that are near to the solubility limit of NaCl in water, a crystal accumulation in near-surface pores during air drying imparts a high strength and brittleness, reversing the reaction-based strength reduction. Analysis of the resulting fracture network by acoustic emission and micro-CT images shows that the fracture characteristics of a brine saturated coal mass vary due to (1) fracture reopening due to coal softening effect during saturation, (2) micro crack initiation and extension/widening of natural cracks due to chemical interactions between coal mass and ions in saturation fluid, and (3) expansion or initiation of cracks during mechanical loading. The strain contour maps and the volumetric deformation analyses infer that the brine saturated coal specimens subjected to mechanical loading exhibit a dilatancy behavior, confirming the higher plastic deformation undergone by the samples due to softer nature and the existence of excessive fractures in the samples. Although the fracture network becomes dense and wide during saturation, the coal mass remains soft and highly deformable, so that mechanically induced fractures may be extensive. This leads to the potential for damaging the rock formation and of contaminating adjacent aquifers. Thus, the design parameters of a stimulation method such as hydraulic fracturing should be carefully determined by considering the pore fluid characteristics, in order to optimize the process and to minimize reservoir damage.

1. INTRODUCTION

Rising energy consumption caused by rapid population growth and industrialization has stimulated the exploration of new unconventional energy resources. In 2016, world total primary energy supply (TPES) was fulfilled by oil (36.0%), natural gas (26.9%), coal (17.1%), nuclear (9.8%), biofuels and waste (5.7%), hydro-power (2.3%), and other renewables (geo-thermal, solar, wind, tide/wave/ocean, heat, etc.) 2.2%.[1] Currently, much attention has been given to replace oil and coal by producing natural gas to surmount the carbon-climate dilemma. Coal bed methane (CBM) is one such source, enabling fuel switching of natural gas to displace the burning of coal. CBM reserves are relatively untapped energy sources with a huge potential to store gas, as they can contain up to seven times the amount of gas stored in a traditional reservoir. The estimated global CBM reserves are about 7500 trillion cubic feet (tcf) with about 1200 tcf in china, 700 tcf in the United States, and 114 tcf in Australia alone. Furthermore, Australia is estimated to hold 8.6% of the world's proven reserves of low rank coal, where United States, Russia, and China hold 28.2%, 23.7%, and 11.5%, respectively.[2] The state of Victoria in Australia has around 430 billion tonnes of brown coal, which has been identified as one of the largest brown coal resources in the world.[3] Victorian brown coal exist in three main basins, namely, Otway, Murray, and Gippsland.[2]

To date, a number of methods have been adopted to extract CBM, mostly associated with the depletion of fluid pressure in the seam, through dewatering.[4] Although these conventional techniques appear simple, they involve many environmental and economic hazards. To overcome these shortcomings, enhanced coalbed methane (ECBM) extraction techniques have been introduced. Hydraulic fracturing is one such practice, which involves introducing a pressurized fluid into the rock formation to generate a network of fractures that facilitate the improved recovery of gas.[5]

The effectiveness and the performance of the hydraulic fracturing process depend on the reservoir properties, fracturing fluid properties, and the in situ conditions. Most potential coal

Received: February 14, 2018
Revised: April 9, 2018
Published: April 12, 2018

ACS Publications © 2018 American Chemical Society

DOI: 10.1021/acs.energyfuels.8b00577
Energy Fuels 2018, 32, 5799−5811

seams are water saturated, and the coal seam gas (CSG) is dissolved in brines containing other mineral constituents. A number of studies have been performed to identify and quantify the chemical and mineral constituents in formation waters associated with CBM in various coal seam reservoirs.[6−11] Van Voast[12] defined the geochemical signature of CSG-infused waters by analyzing the hydrochemistry of CSG for different coal reservoirs in the United States. The signature consists of high Na^+ and HCO_3^- concentrations, low Ca^{2+} and Mg^{2+}, and negligible SO_4^{2-} concentrations. The variations in CSG water chemistry in 31 groundwater samples taken from coal seams in Maramarua, New Zealand, have been analyzed by Taulis and Milke.[13] They identify that similar to Van Voast[12] results, the CSG water has high concentrations of Na^+ (334 mg/L), Cl^- (146 mg/L), and HCO_3^- (435 mg/L) and low concentrations of Ca^{2+}, Mg^{2+}, and SO_4^{2-} concentrations. Further, this water has high alkalinity (360 mg/L as $CaCO_3$) and pH 7.8, as a result of biogenic processes and dissolution of carbonate. NaCl concentrations in CSG water can severely affect the mechanical properties of the rock formations. Studies on the detrimental effects of brine saturation on rock properties show that brines with different ionic strengths cause irreversible formation damage to reservoirs.[14−18]

Understanding the mechanical behavior of rock formations saturated with pore fluids with different ionic concentrations is thus important when designing a hydraulic fracturing project. Typically, the modeling of hydraulic fracturing is performed to determine the desired pumping schedule, operating parameters and the expected breakdown pressure. Most conventional models assume linear elastic response, the propagation of a planar fracture and, constant permeability.[19] However, the alteration of mechanical properties, such as compressive and tensile strength, Poison's ratio, brittleness, Young's modulus, and fracture gradient due to different saturation conditions can affect the performance of the hydraulic fracturing process. Among the various properties, brittleness is a rock property widely used in rock engineering applications to interpret the failure characteristics of a particular rock formation.[20] It is assumed that a brittle rock formation can be easily fractured through shear or tensile failure modes, where the generated fracture network have a higher potential to be retained open by proppants.[21,22] However, this assumption is not always true since some rock formations with higher brittleness can act as a fracture barrier and might be a poor candidate for fracturing.[23]

Although, numerous studies have been conducted on different rock samples to interpret strength variations and fracture characteristics under different brine saturations, coal seam mechanical behavior is not widely discussed referring to the induced fracture characteristics. Since coal is a unique rock type with high organic content, the coal mass−brine interaction can significantly alter the reservoir properties. This paper provides a comprehensive experimental study on the interpretation of the alteration of coal seam mechanical properties and induced fracture characterization under different brine saturations to address the effective evaluation of the hydraulic fracturing process. The study consists of the evaluation of mechanical properties (Uniaxial compressive tests) along with ARAMIS photogrammetric analysis, acoustic emission (AE) analysis, microcomputed tomographic (micro-CT) analysis, scanning electron microscopy (SEM), and chemical analysis, in order to define the variation of mechanical behavior in coal under different brine saturations.

2. EXPERIMENTAL PROCEDURE

2.1. Characteristics of Brown Coal Samples. The brown coal samples were collected from the Loy Yang mine, Latrobe Valley, Victoria, Australia. The brown coal has a high moisture content, ranging from 50% −70% by weight. The coal seams are often only 10−20 m below the ground surface and can be up to 100 m thick, sometimes increasing to 230 m where multiple seams coalesce.[24] Typical characteristics of Latrobe valley brown coal are mentioned in Table 1. The collected brown coal samples have average bulk density and dry density of 1130 kg m^{-3} and 700 kg m^{-3}, respectively. The approximate specific gravity of the samples is ∼1.13, and the gravimetric porosity is ∼0.37.

Table 1. Typical Characteristics of Latrobe Valley Brown Coal[24,25a]

coal seam characteristic			typical values
energy value (gross dry)			25 MJ/kg to 29 MJ/kg
energy value (net wet)			5.8 MJ/kg to 11.5 MJ/kg
coal: overburden strip ratio			0.5:1 to 5:1
results of ultimate and proximate analyses	carbon	wt %, d.a.f.	65% to 70%
	hydrogen	wt %, d.a.f.	4% to 5.5%
	nitrogen	wt %, d.a.f.	0.5%
	oxygen (by diff)	wt %, d.a.f.	25% to 30%
	fixed carbon	wt %, d.a.f.	47.7%
	volatile matter	wt %, d.a.f.	52.3%
	ash	wt %, d.a.f.	1.5%
	moisture	wt %, a.r.	59.4%

[a]d.a.f., dry ash free; a.r., as received; diff., difference.

2.2. Sample Preparation. Congruent with ASTM standards, the brown coal samples were cored and trimmed (length of 76 mm and diameter of 38 mm) using coring and cutting machines in the Deep Earth Energy Research Laboratory (DEERL) of Monash University. Both ends of the samples were ground to achieve parallel, flat, and smooth surfaces using a grinder to ensure a uniform load distribution. The salinity of CSG water is typically measured as the concentration of total dissolved solids (TDS), and the natural brine concentration of a typical coal seam gas reservoir varies from 0.2−12.5% by weight.[26] Thus, brine saturation concentrations for this study were chosen by considering the natural brine concentrations of typical coal reservoirs and also to cover a broad range to clearly differentiate the results. Three brine saturations (i.e., 0%, 10%, and 20% NaCl by weight) were selected to saturate the prepared brown coal samples. Three samples were tested at each concentration and all the samples were saturated for 3 months in desiccators under vacuum, in order to achieve fully brine saturated conditions. Starting from the beginning of saturation, the weight of a representative core sample was measured continually over time to make sure that the samples become fully brine saturated by the considered time period. The weight measurement was continued until the sample weight gradually became constant, which implied that the samples were fully saturated.

2.3. Uniaxial Compressive Strength (UCS) Test. Once the samples were fully vacuum-saturated, nine uniaxial compression tests (UCS) were completed to quantify and analyze the mechanical alteration resulting from brine saturation conditions. A Shimadzu AG9 uniaxial compression machine, which has a maximum capacity of 300 kN was used to perform the UCS tests. Congruent with ASTM standards,[27] a compression loading rate was selected, such that the sample failure occurs in a test time between 2 and 15 min. In accordance with this specification, the loading rate was applied at a rate of 0.1 mm/min, and the applied load and displacement history were recorded with an advanced data acquisition system (see Figure 1).

DOI: 10.1021/acs.energyfuels.8b00577
Energy Fuels 2018, 32, 5799−5811

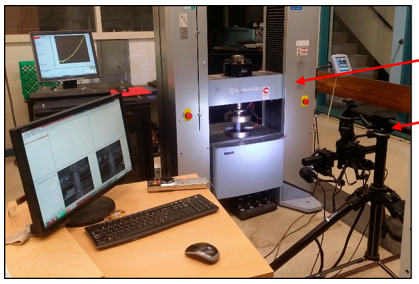

Figure 1. UCS tests were performed in Shimadzu AG9 compression machine and the axial and lateral stains were captured with ARAMIS 3-D deformation measuring system.

2.4. ARAMIS Photogrammetric Analysis. The corresponding axial and lateral strains were recorded using ARAMIS photogrammetric equipment (a noncontact optical 3D deformation measuring system) (see Figure 1). The speckle images were captured in pixel format with two highly sensitive cameras and the structural deformations were recorded by tracing the discrete correlated areas within the stereo images. To unequivocally match the correlated areas within the dual captured stereo images, the samples require satisfactory variations in tone and contrast. In order to accomplish that the samples were air-dried to achieve a surface dry condition and the surfaces were painted with flat white paint and then matt black dots were sprayed over the sample surface. The images were filtered using the ARAMIS software and the strains during the sample deformation were analyzed using a noncontact optical 3-D metrology system.

2.5. Acoustic Emission (AE) Analysis. The acoustic emission (AE) monitoring was used to identify fracture propagation in the coal samples during load application. The AE system consists of a PCI 2-channel data acquisition system, which has a nominal resonant frequency of 500 kHz and a band-pass filter with a frequency ranging from 250 kHz to 750 kHz. In each test, three sensors were attached to the basal plate of the compression machine and an electron wax was used on the sensors to obtain the same sensitivity. The low frequency acoustic waves generated during the fracture propagation were magnified using amplifiers, which were set to 40 dB to amplify the resulted AE signals.

2.6. Microcomputed Tomography (Micro-CT) Analysis. Micro-CT analysis was performed to analyze the fracture distribution in samples after mechanical failure during the UCS test. Full size coal samples of 38 mm diameter and 76 mm length were scanned in the Australian Synchrotron imaging and medical beamline (IMBL) facility. Three representative samples (i.e., each from 0%, 10% and 20% saturation concentrations) were scanned after the UCS tests and the induced fracture networks at failure, due to uniaxial compressive loading, were visualized and quantified with AVIZO image analysis software. The fracture distribution and characteristics, such as fracture density and fracture aperture at each brine concentration are described together with the results of the AE and ARAMIS analyses. Imaging parameters and specification of the micro-CT instrument used for this study are given in Table 2.

2.7. Chemical Analysis. In order to identify the chemical constituents contained in the natural and brine saturated coal samples used in the study, an energy dispersive spectrometry (EDS) analysis was carried out at the TrACEES platform, geology node, University of Melbourne. The system is an Oxford Inca, which consists of an ATW2 thin detector window and a liquid-nitrogen cooled Si–Li detector, allowing the X-ray collection between B and U. The scanning was focused on a selected area of natural and brine saturated coal fragments (see Figure 2) and the obtained results were used to discuss the chemical reactions occurring in the coal mass due to different brine concentrations. Further, X-ray diffraction (XRD) analysis was carried out at the Materials Characterization and Fabrication Platform (MCFP), University of Melbourne, to identify the mineral composition of the coal samples.

Table 2. Imaging Parameters and Specification of the Micro-CT Instrument Used for the Study

scanning parameters	specifications
research facility	Australian Synchrotron imaging and medical beamline (IMBL) facility
detector	ruby with 150 mm lens and 20 μm screen
sample size	38 mm (diameter) × 76 mm (height)
voxel size	16.73 μm
acquisition time	20 min
energy of X-ray	40 keV
no. of projections	3 segments per sample, 1800 projection per each segment
detector to sample distance	1.4 m
filter	none

3. RESULTS AND DISCUSSION

The obtained results from each analysis enable to draw important conclusions on the effect of brine saturation concentrations on brown coal. The results are discussed under three categories: (1) chemical interactions occur under different brine concentrations, (2) alteration of mechanical properties (i.e., strength, brittleness, and deformation behavior), and (3) fracture propagation and distribution at failure, due to each brine saturation condition.

3.1. Possible Chemical Interactions Occur under Different Brine Concentrations. The energy dispersive spectrometry (EDS) analysis is an analytical technique used for the chemical characterization and qualitative elemental analysis of a sample. Two EDS analyses have been carried out on natural and brine saturated representative samples to identify the chemical constituents contained in the samples. Knowledge of the chemical elements that contribute to coal–brine interaction is important to define the characteristic variation of coal samples in each saturation condition. Figure 2 illustrates the major constituents contained in each sample. The results from the natural sample (see Figure 2a) show that except for carbon (C) and oxygen (O), there are no significant secondary chemical constituents in the coal sample used for this study. Conversely, the brine saturated sample includes sodium (Na) and chlorine (Cl) (see Figure 2b), imbued from the saturating brine. This result is further confirmed by conducting an XRD analysis on a natural coal sample in order to identify any major minerals contained in the sample. As shown in Figure 3, the analyzed data show only a two peaks in the natural sample, so it is not possible to conclusively define what mineral phases are present. Studies show that the total mineral content of the brown coal is often less than ∼2%; therefore, the concentration of individual minerals would be less than ∼1%, which is below the detection limits for XRD.[28,29] Thus, it can be concluded that the characteristic variation of the coal samples is mainly governed not by the interactions between minerals (formed by other chemical constituents) and brine, but by the interactions between the coal mass (carbon and oxygen) and the brine itself. Based on this conclusion, the results in this study are discussed by considering the coal mass–brine interaction.

Low-rank Australian brown coals are normally rich in oxygen containing groups such as phenolic hydroxyl and carboxyl groups, which are known as surface functional groups with cation exchange properties.[30] Many researchers have proposed different ion exchange mechanisms in coal masses, which are generally dependent on temperature, additives, solid to liquid

DOI: 10.1021/acs.energyfuels.8b00577
Energy Fuels 2018, 32, 5799–5811

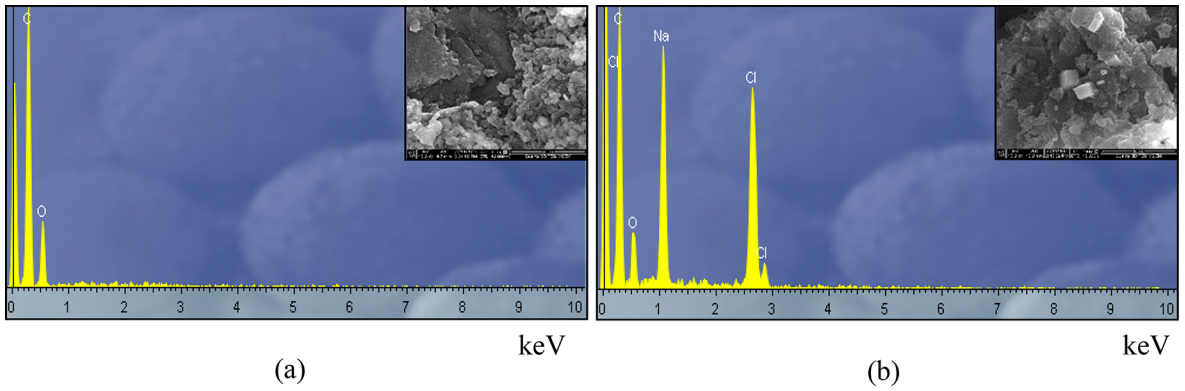

Figure 2. Results from SEM/EDS analysis showing major elements contained in (a) the natural coal sample and, (b) the brine saturated sample used for the study.

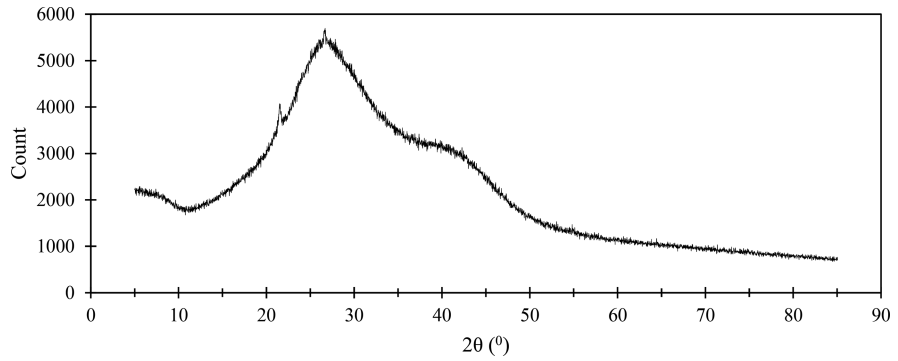

Figure 3. Results from XRD analysis of natural coal sample, showing only two minor peaks, indicating that there is no considerable mineral composition in the brown coal sample.

ratio, and pH.[30,31] Domazetis and James[32] developed a brown coal model for interaction with NaCl. They note that the model is stabilized when the cations are located in spaces that reduce steric hindrance and are surrounded by water molecules and oxygen functional groups. As explained in this study, one possible interaction between brine and coal mass is once the brine is introduced to the coal mass, they act separately as water molecules, Na^+ cations, and Cl^- anions. The water molecules form H-bonds with oxygen functional groups, whereas cations are placed within the coal molecular structure, adjacent to carboxyl anions to resemble a base/acid reaction. The reaction depends on the characteristics of the brown coal and the ionic concentration, which ultimately govern the alteration in coal structure.

The change in the pH of the solution before and after saturation of the brown coal samples was measured (see Figure 4). Since, the addition of NaCl into distilled water does not change its pH value, the solution pH at each NaCl concentration was maintained at pH ~7. However, the solution pH significantly drops after the full saturation of the coal samples, becoming acidic. As described by Fuerstenau et al.,[33] when coal is immersed in a liquid, a charge develops on the surface by dissociation of functional groups (COOH, C═O, COH) from the surface or by adsorption of ions from solution. Since, the lower rank coal contains a greater fraction of oxygen functiona1 groups, they provide additional negatively charged sites on the surface of the coal. Simultaneously, the dissociation of acidic oxygen functional groups release H^+ ions to the solution, resulting an acidic environment (see eq 1). Further, the decreased pH due to the NaCl concentration indicates that the acidity of the solution has been increased with increasing

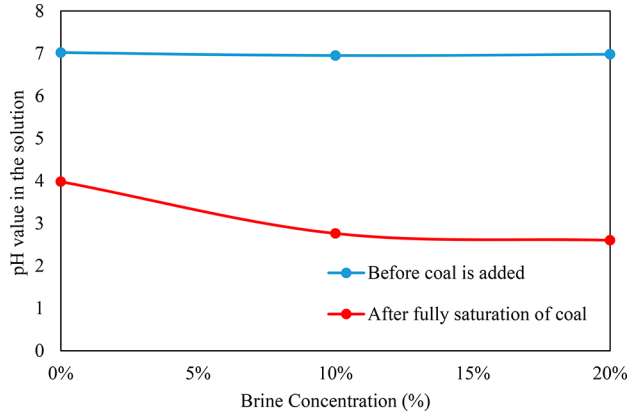

Figure 4. Variation of pH with NaCl concentration in the saturating solution both before and after coal saturation. Note that the samples were immersed in a constant volume of solution and the pH values were measured at room temperature of 26 °C.

brine concentration. This is because, when Na^+ cations are introduced to the solution, the interaction between oxygen functional groups and cations releases more H^+ ions, resulting a more acidic environment (see eq 2).[31] The pH of a solution is an important parameter for evaluating the corrosiveness of a chemical reaction. According to Langmuir,[34] the severity of corrosion tends to be greater under high-pH or low-pH conditions than at near neutral-pH values. This is due to the effect of H^+ and OH^- ions in acidic and alkaline environments, respectively, which form surface active complexes that destabilize the stable internal bonds, resulting in release of

DOI: 10.1021/acs.energyfuels.8b00577
Energy Fuels 2018, 32, 5799−5811

Table 3. Results of Uniaxial Compressive Strength (UCS) and Brittleness Index (BI) Obtained from Stress-Strain Curves for Each Brine Saturation Concentration

saturation (%)	sample	UCS (MPa)	avg UCS (MPa)	ΔUCS (%)	BI (%)	avg BI (%)	ΔBI (%)
	01	0.693			61.65		
0	02	0.761	0.712 (SD = 0.043)		65.71	65.05 (SD = 3.12)	
	03	0.682			67.78		
	01	0.439			73.22		
10	02	0.418	0.423 (SD = 0.014)	−40.6	73.93	71.42 (SD = 3.74)	9.8
	03	0.4126			67.12		
	01	0.741			77.69		
20	02	0.651	0.737 (SD = 0.084)	3.6	77.45	77.13 (SD = 0.78)	18.6
	03	0.82			76.24		

cations at low pH and anions at high pH environments. Thus, the severe corrosive reactions triggered under low-pH values (at high NaCl concentrations) can cause significant strength reductions in coal mass.

Even though, this particular coal type does not contain a significant mineral composition, the dissolution of minerals in mineral-rich reservoirs under acidic environment can also cause a significant strength reduction in the rock mass. Labus and Bujok.[35] analyzed the mineral dissolution mechanisms and capacity of the upper Silesian coal basin and found that the dissolution of calcite or siderite in favorable acidic environments is a typical reaction in the particular aquifer, which contains carbonate minerals in its rock matrixes. This reaction increases the carbonate concentration in pore water and may enhance the kaolinite dissolution due to increased acidity. Dissolution of such minerals significantly affects the grain-to-grain contacts in the reservoir rock and reduces the bond energy of the pore structure, resulting in a strength reduction.[36] For instance, Rathnaweera et al.[18] showed that the mechanical strength of a brine saturated rock mass can be significantly reduced due to dissolution of carbonate minerals such as calcite and siderite. Also the dissolution of pore filling calcite weakens the rock mass pore structure by creating a secondary porosity system within the primary pores.[37] Therefore, the dissolution of minerals in high acidic environments is also an important factor, which should be carefully evaluated, considering the reservoir mineralogy.

$$(\text{coal}-\text{COOH}) \rightleftharpoons \text{coal}-\text{COO}^- + \text{H}^+ \quad (1)$$

$$(\text{coal}-\text{COOH}) + \text{M}^+ \rightleftharpoons \text{coal}-\text{COOM} + \text{H}^+ \quad (2)$$

3.2. Alteration of mechanical properties due to different brine concentrations. The stress−strain relationships obtained from UCS tests provide an indication of stiffness and strength. In this study, the stress−strain curve is used to determine the average uniaxial compressive strength and brittleness index of coal samples under each brine concentration. The results are illustrated in Table 3 and Figure 6. Different authors use the term "brittleness" differently with no apparent uniform definition. Current methods to define brittleness include stress−strain, reversible energy, Mohr envelope, compressive strength, tensile strength, and macro- and microhardness based approaches. This study uses the stress−strain based approach (see Figure 5) as it has been found to be suitable for friable materials like coal.[38] The brittleness index is defined in this approach as

$$\text{brittleness index (BI)} = \frac{\text{reversible strain}}{\text{total strain}} = \frac{\text{DE}}{\text{OE}} \quad (3)$$

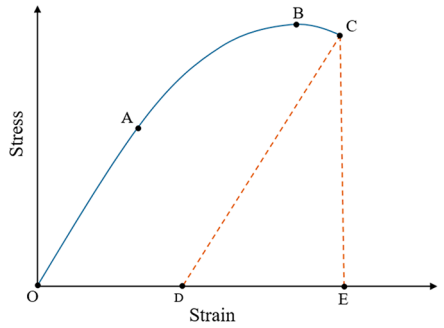

Figure 5. Determination of brittleness index from the stress−strain based approach (refer eq 3).

The results of the UCS tests performed on coal samples indicate that the change in the brine concentration of the pore fluid causes significant alterations in mechanical properties. The nonmonotonic variation (U shaped curve) of average UCS vs brine concentration shown in Figure 6 illustrates that there is

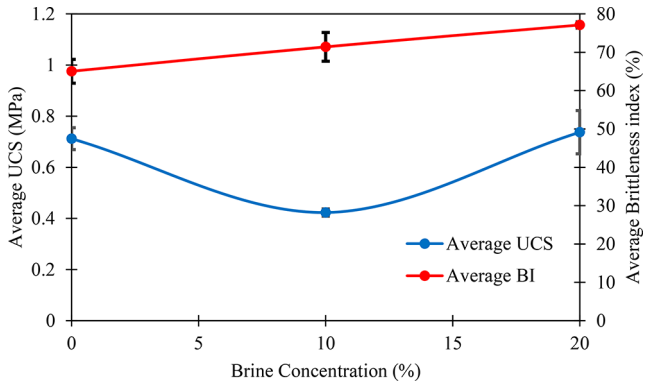

Figure 6. Variation of average uniaxial compressive strength (UCS) and average brittleness index (BI) with brine concentration.

no simple or direct relationship between two parameters. Previous studies on different rock types show different trends between rock mechanical strength and pore fluid ionic concentration. Rathnaweera et al.[15] noted that the stress−strain behavior of rock specimens from a deep saline aquifer change significantly with the change in brine concentration of the pore fluid. Feucht and Logan[17] showed that mechanical weakening in reservoir rocks can be significant at high and low ionic strengths of the pore fluid, and mechanical strengthening may occur at intermediate ionic strengths. Conversely, Shukla et al.[16] found a "U shaped" relationship between rock strength and salinity (NaCl %), where the strength initially reduced and

DOI: 10.1021/acs.energyfuels.8b00577
Energy Fuels 2018, 32, 5799−5811

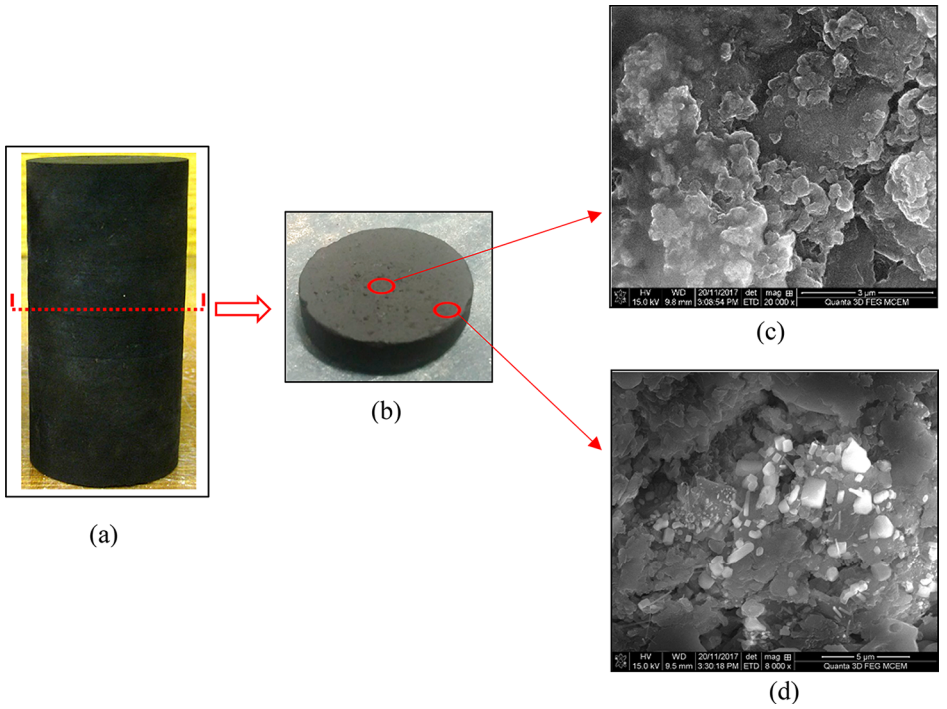

Figure 7. Results of SEM analyses conducted on two fragments obtained from a thin coal slice (b) cut from a fully brine saturated (20%), air-dried core sample (a). (c) Image of interior pore structure indicating no crystal accumulation in inner-pores and (d) image of pore structure near to sample surface, indicating an excessive crystal accumulation in outer-pores. Note: Analyses were carried out under same scanning parameters, which are 15 kV voltage with a 4.5 spot size and 9.5 mm working distance.

then increased with increasing NaCl concentration. The results of this study are in line with most of the past literature, and it infers that the complex formation of coal subjected to varying brine saturation concentrations can result unpredicted strength evolution.

Viete and Ranjith[39] found that the average unconfined compressive strength of an air saturated sample from the same coal mine was around 0.966 MPa. The water saturated (i.e., 0% brine concentration) samples of this study have a lower average UCS strength of 0.712 MPa, than the air saturated sample strength, which implies that the lower strength (i.e., 26.2% strength reduction) is caused by coal softening by water. This observation agrees with Perera et al.,[40] who conducted mechanical tests on the same Latrobe valley brown coal and found a 17% stress reduction due to coal softening. The reduction of this overall strength may result from water molecules reacting with the mineral and clay content in the rock samples that consequently soften the bond structure.[41] In fact, Van Eeckhout[42] has comprehensively studied the mechanisms of strength reductions due to moisture in rock. As identified in this study, the strength reduction basically depends on five factors, namely, (1) reduction of fracture energy, (2) reduction of capillary tension, (3) pore pressure increase, (4) frictional reduction and, (5) chemical and corrosive deterioration. The pore pressure is an important factor, which affects the strength of rock with interconnecting pore structure and controlled by the effective stress. If the pore fluid in the saturated coal mass is pressurized during loading, an outward pressure gradient would be created, lowering the strength. Furthermore, Lama and Vutukuri[43] suggested that the interaction of moisture with the rock mass can reduce the surface energy, resulting in a significant strength reduction. However, the influence of each factor on the overall strength reduction may depend on the rock type and the loading conditions. Except these factors, water adsorption into a coal mass causes a significant swelling effect, resulting an alteration in coal microstructure. This was confirmed by Zhang et al.[44] as they have imaged a coal plug before and after brine saturation and found that more than 80% of cleats closed due to swelling. The swelling effect may be another reason for coal strength reduction, as the coal matrix swells and becomes relax due to decreased capillary pressure and enlarged volume, after water saturation. The swelling induced strength reduction was studied in nanoscale by Zhang et al.,[45] in which they compared the elastic moduli of a coal sample measured by nanoindentation tests and found that indentation moduli of the coal sample has been decreased by 60−66% after the water adsorption. Thus, it is evident that there are several causative factors that affect the strength of a water saturated coal mass, and a deep investigation of the influence of each factor is important, when evaluating the coal mass mechanical property alterations.

Interestingly, at 10% brine concentration, the overall strength of the sample has greatly reduced. In fact, the strength reduction from water saturation to 10% brine concentration is as high as 40.6%. This implies that in the case of 10%, the high ionic concentration in the solution triggers chemical interactions between the pore fluid and the coal mass, resulting in a low strength. The observed low pH (2.76) indicates that the coal mass and brine solution have undergone a significant chemical reaction, resulting a more acidic environment (see Figure 4) and thus a strength reduction. Johns et al.[46] illustrated the variation of compressive strength of densified brown coal as a function of pH and showed that the compressive strength decreases with decreasing pH. Moreover, the nature of this strength reduction with increasing brine saturation has been observed by many researchers. Feucht and Logan[17] showed that

DOI: 10.1021/acs.energyfuels.8b00577
Energy Fuels 2018, 32, 5799−5811

(a) 0% brine concentration (b) 10% brine concentration (c) 20% brine concentration

Figure 8. Crystal accumulation on sample surface of air-dried samples (saturated with brine for 3 months and exposed to atmosphere for 24 h).

friction in rock decreases due to the ionic concentration of NaCl and the rock strength reduces due to the corrosive nature of the chemical reactions between the rock structure and brine. Dunning and Miller[47] concluded that for relatively friable rocks, an adequate chlorine-rich ionic concentration of chemical solutions weakens rocks over the case of with distilled water alone. A hypothesis proposed by Swolfs[48] suggests that a reduction in rock mass strength may result due to the adsorption of ions or molecules on to the rock surface, resulting in a reduction of the free surface energy of the rock.

At 20% brine concentration, the coal strength has again increased from 0.423 MPa at 10% concentration, up to 0.737 MPa, corresponding to an increment of 74.2%. The trend reversal with increasing brine concentration or the 'U' shape trend suggests that there should be another mechanism that involves to overcome the reaction-based strength reduction. The results are in accordance with study completed by Shukla et al.,[16] as they suggest that, when increasing the brine concentration, the softening effects of the rock mass are dominated by the NaCl crystallizing effect in the rock pores. However, this argument might not accurate, because the brine concentrations used for the study (maximum of 20% or 200 g/L) are less than the solubility limit of NaCl in water (approximately 360 g/L at 26 °C). Therefore, no crystal accumulation can be expected in coal pores during the saturation period, because all the NaCl added to the solution remain dissolved due to low ionic concentration. However, in this case, some crystal formation can be anticipated in near-surface pores due to air drying of the samples before testing. In the testing procedure, the samples were air-dried before UCS testing, because as explained in section 2.4, the sample surfaces had to be preprepared for ARAMIS analysis. Desorption or evaporation of moisture from the external surfaces of coal samples is always faster than desorption from the interior during drying,[49] and air drying removes most of the surface moisture of the coal. Therefore, the degree of saturation of a sample exposed to atmosphere varies, with having a high moisture content at inner-pores but low or no moisture in near-surface pores. In concurrence, some NaCl crystals can be accumulated in pores near to sample surface during the shorter drying period, while NaCl in the inner-pores remain dissolved.

To test this hypothesis, we conducted two SEM analyses on a coal sample saturated at 20% concentration. The fully saturated coal sample was air-dried for a similar time period as UCS tested samples and a thin slice was cut from the sample. The SEM analyses were carried out under same scanning parameters on two coal fragments obtained from two locations of the parent sample (i.e., one fragment from near surface of the parent sample and the other from inside of the sample). As expected, there were no crystals visible in the coal fragment obtained from inside of the coal mass, which confirms that no crystal accumulation has taken place in interior pores, during the saturation or short drying period. In contrast, a significant crystal accumulation was observed in the fragment obtained from near-surface (see Figure 7), which has been caused by moisture removal from the exterior pores. In order to differentiate the variation of crystal accumulation with brine concentration, three coal fragments were saturated at 0%, 10%, and 20% brine concentrations and kept in atmosphere (subjected to air drying) for 24 h to allow crystal formation on the samples. As illustrated in Figure 8, an excessive crystal accumulation on the surface of the coal fragment at high brine concentrations (i.e., 20%) can be clearly visualized with the naked eye. The sample surface was almost covered with crystals at 20% concentration, while no visible crystal formations were observed at 0% and 10% cases. The results imply that only high order of brine concentrations, closer to solubility limit, has formed crystals in the sample during the 24 h of the air drying period.

The crystal accumulation during the drying period should be the reason for the strength increment at high brine concentrations, as observed in this particular study. This implies that, at 20% concentration, although the corrosive chemical reactions occurred due to high ionic concentration and at favorable pH environment, the considerably higher crystal accumulation in near surface-pores have overcome its effect, giving a high strength to the sample. However, it should be noted that the crystal accumulation occurred not during the saturation period but due to the surface drying. However, under actual reservoir conditions, the maximum NaCl concentration reported in CSG water is around 0.2−12.5%,[26] and around 90% of coal reservoirs remain saturated and are not subjected to air drying. Therefore, crystal accumulation based strength regains cannot always be anticipated in underground reservoirs, because the NaCl in CSG water remains dissolved, unless the concertation exceeds its solubility limit or the reservoir is subjected to a low degree of saturation due to reasons like depletion of the water table. Furthermore, it should be highlighted that in any case, the laboratory experiments does not 100% replicate the actual reservoir conditions, especially for coal, due to its larger heterogeneity and stress sensitivity. The different core samples may exhibit different strengths or failure points/patterns during mechanical loading, even though they are drilled from the same coal block. A careful attention should also be given when preparing the brown coal samples (during coring, cutting, and grinding), as they can be easily disturbed due to the softer nature. We have tested three core samples per each saturation condition and obtained quite reasonable results in terms of unconfined compressive strength (see Table 3). However, if there is more heterogeneity observed in the tested samples, one should test more samples in each condition, in order to get more reasonable and reliable results. Furthermore, the samples were tested after 24 h of air drying period, which was necessary for ARAMIS photogrammetric analysis. The air

DOI: 10.1021/acs.energyfuels.8b00577
Energy Fuels 2018, 32, 5799−5811

drying of the samples, even for such shorter period might cause a deviation of results from fully saturated conditions. Therefore, it is highly recommended to evaluate the mechanical property alterations under fully saturate conditions to simulate the actual reservoir conditions.

3.3. Fracture Propagation and Distribution in Each Saturation Concentration. The fracture initiation, propagation, and distribution within the coal samples that develop during saturation and loading vary and thus, the sample deformation vary due to structural alterations resulting at each NaCl saturation. In this study, the combined results of three monitoring and characterization methods, namely, acoustic emission (AE) analysis, ARAMIS photogrammetric analysis, and micro-CT image analysis are used to clarify mechanical deformation of samples under uniaxial loading and to characterize the resulting induced fracture network.

Any material subjected to compressive or tensile loading, sustains changes in the rock structure by closing, or initiating and propagating new microfractures.[50] Acoustic waves are a form of strain energy released during this process. The spontaneously generated acoustic signals provide indirect information on micro cracking such as fracture size, fracture initiation time, fracture density, and deformation mechanism. Monitoring the acoustic emission (AE) count during load application is a routine method to analyze fracture initiation, propagation, and damage in a brittle rock mass. This has been widely used by many researchers to interpret crack generation processes in rock masses being subjected to compression or tension. The trend of cumulative AE count throughout the application of load has been explained by Ranjith et al.[51] by separating it into three main stages, namely, (1) crack closure, (2) stable crack propagation, and (3) unstable crack propagation. No AE events are observed at the beginning of the load application, and the rock mass is considered to be in its crack closure stage. The very first AE event indicates the crack initiation point. Once cracks are initiated, a gradual increase in AE energy release is observed with the progressive load on the rock specimen- this indicates the stable crack propagation period. Further increase in the load exhibits an exponential increase of AE energy release, which is caused by the unstable crack propagation. This stage creates a significant damage in the sample until the eventual failure. Referring to this interpretation, in this study, the cumulative AE energy has been measured beginning from load application and followed until failure. This is plotted with the axial strain in Figure 10 and used to identify various failure stages of each sample.

"Digital image correlation" (DIC) is often used to obtain full-field strain profiles of materials subjected to loading rather than determining localized strain measurements.[52] ARAMIS is a material independent, noncontact measuring system based on DIC, which has the capability of full-field analyses of test specimens. ARAMIS image analysis continuously captures the strain variation of rock samples, subjected to continuous loading.[15,53−55] Both vertical and horizontal strain measurements over the entire sample at a particular time interval provide information on how the samples deform in both directions during external load application. The simplest way of visualizing and comparing the strain distribution is by using the strain-contour maps for samples at a common scale. The strain distribution contour maps of representative samples from each brine saturation concentration have been used in this study to quantify the strains and deformations undergone by the samples prior to failure (see Figure 12). Also, the volumetric strain−stress curves are often used to interpret the deformation mechanisms and microscopic activities of rocks. Three patterns of deformation have been identified in samples subjected to uniaxial loading, namely, (1) dilatancy, (2) compaction, and (3) dilatancy followed by compaction. For the analysis, the lateral and axial strains are defined as negative for expansion and positive for compression, and the volumetric stains were calculated according to eq 4. Figure 13 illustrates the variation of volumetric strain with respect to axial stress, and is used for the comprehensive interpretation of the sample deformations under uniaxial loading.

$$\text{volumetric strain } (\varepsilon_v) = \text{axial strain } (\varepsilon_a) + 2\cdot\text{lateral strain } (\varepsilon_l) \quad (4)$$

X-ray micro computed tomography (micro-CT) is a rapid nondestructive technique used to yield three-dimensional X-ray images of solid specimens including various geological materials.[56] Micro-CT images were used for evolution of the coal structure, fracture characterization, evaluation of permeability alteration at different pressures, analysis of coal damage under external loading, and evaluation of coal heterogeneity covering the distribution of minerals, pores, and fractures.[45,57−60] The micro-CT technique has the capability of providing enhanced resolution 3D images allowing for digital isolation, visualization, and quantification of favorable sections in the core sample.[60] Based on this key advantage, full scale scanning of the 38 mm × 76 mm core samples have been carried out in this study to characterize the propagated fracture network. The quantification of the induced fracture network in each saturation condition was conducted using image segmentation method in cooperated with micro-CT 3-D reconstructed data of representative samples (see Figure 9). The induced fracture density and the fracture aperture details of failed samples were visualized and quantified and are given in Figure 11 and Table 4, respectively.

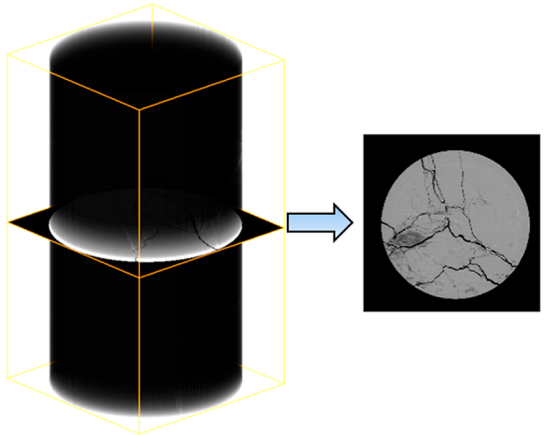

Figure 9. 3-D reconstruction of full scale failed sample for fracture quantification and the extraction of a representative ortho-slice for the fracture visualization.

As shown in Figure 10a, the total cumulative AE count when water saturated (i.e., 0% brine saturation) has a very low count of 135 at failure, indicating that no significant fracture propagation occurred during the load application. The crack closure time is high, where the first crack initiated almost halfway through the load application. The micro-CT image

DOI: 10.1021/acs.energyfuels.8b00577
Energy Fuels 2018, 32, 5799−5811

Table 4. Results from the Micro-CT Image Based Quantitative Analysis of Induced Fracture Networks

Saturation concentration	Total volume of fracture network (μm^3)	Fracture density (= fracture volume / total volume) %	Average fracture aperture (mm)			
			min	avg	max	Aperture range
0%	8.16E+11	1.24	0.082	0.298	0.435	0.082 0.298 0.435
10%	1.38E+12	2.11	0.032	0.281	0.446	0.032 0.281 0.446
20%	1.76E+12	2.65	0.0049	0.151	0.372	0.0049 0.151 0.372

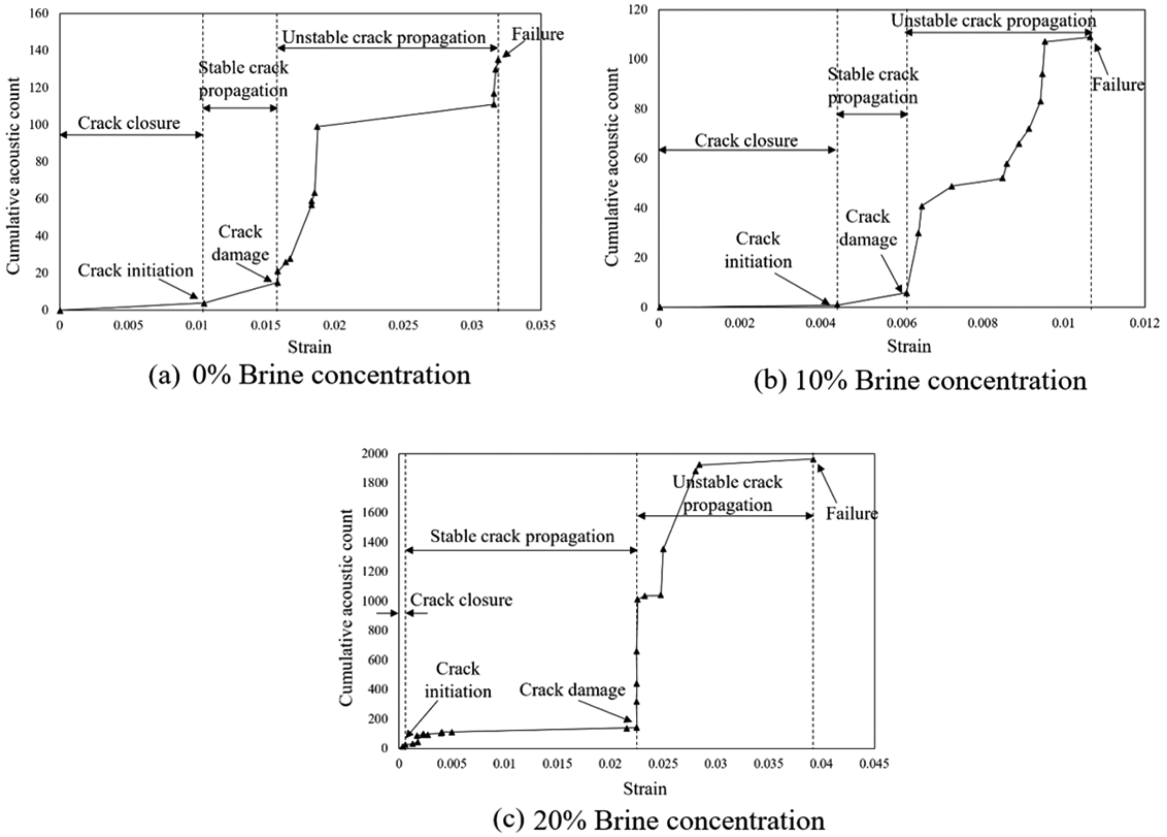

Figure 10. Variation of cumulative acoustic emission (AE) count with axial strain of samples during the load application.

analysis of the same condition also shows a low fracture density (i.e., 1.24%) in the corresponding sample (see Table 4). However, the observed fractures are quite extensive and not much thinner (see Figure 11a), where the minimum fracture aperture is 0.082 mm, the highest among the three conditions (see Table 4). Since AE count is too low, it can be concluded that the observed extensive and thicker fractures may be induced not during the UCS loading, but during the saturation period. The higher fracture aperture in the micro-CT image based quantification implies that the natural fractures are subjected to fracture reopening and widening during the water saturation. This observation is consistent with many studies of coal softening and fracture reopening during water saturation.[40,41,43] Lama and Vutukuri[43] explained that natural fractures in a coal mass may extend as the moisture inside the rock is easily attached to the natural fracture tips by creating stress corrosion at the tip and dissolving the material. Moreover, the large strain distribution in the ARAMIS color map (see Figure 12a) suggests that the sample has been subjected to a considerable plastic deformation prior to failure, which might be another reason for the higher fracture aperture, as the samples have undergone a large deformation before failure, widening the induced fracture network. The volumetric strain variation exhibits a compaction followed by a dilatancy behavior, which also confirms the nonelastic deformation of the sample, caused by the softer nature and the volume expansion due to fracture opening under compressive loading (see Figure 13).

DOI: 10.1021/acs.energyfuels.8b00577
Energy Fuels 2018, 32, 5799−5811

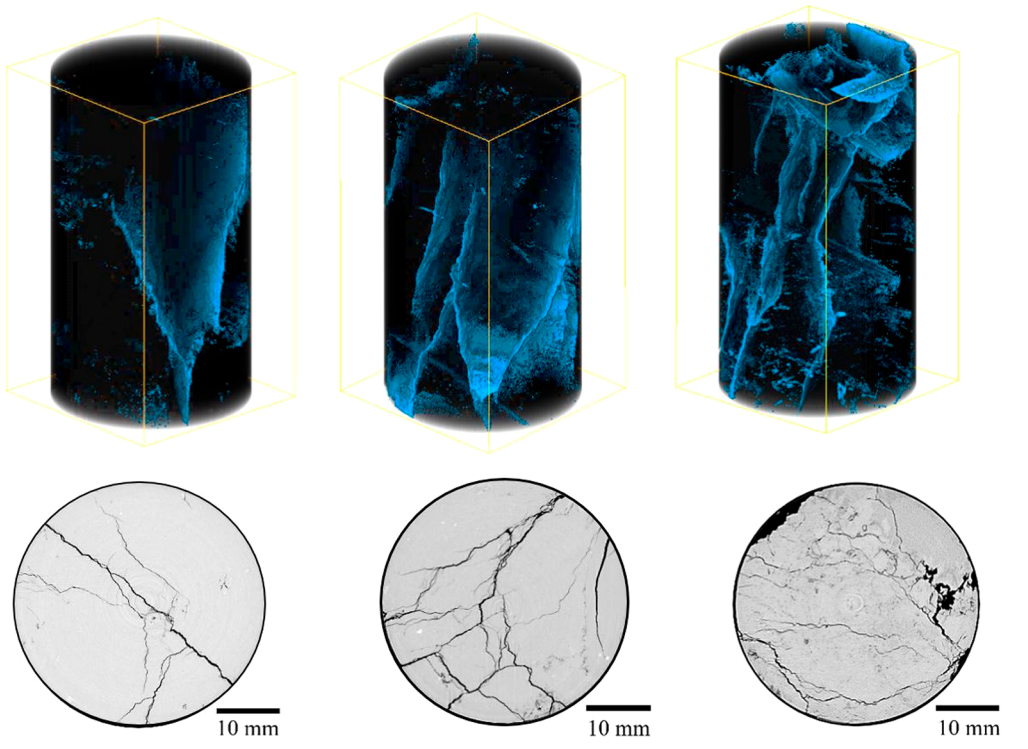

Figure 11. 3-D visualization of the induced fracture network at full scale based on micro-CT image data and the typical cross sections at each sample to clearly visualize the fracture aperture and pattern.

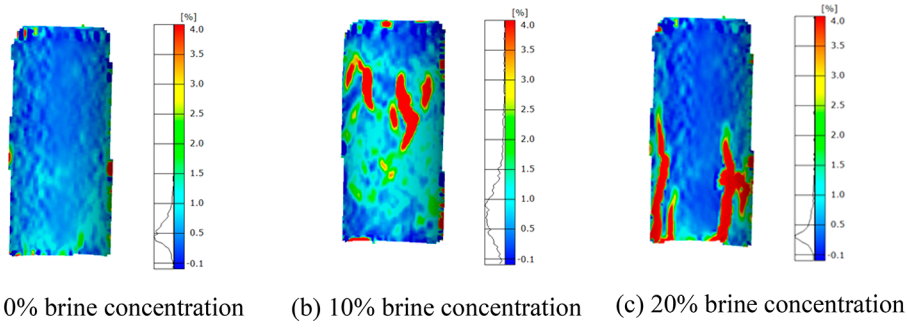

Figure 12. Strain distribution contour maps of representative samples from each brine saturation concentration.

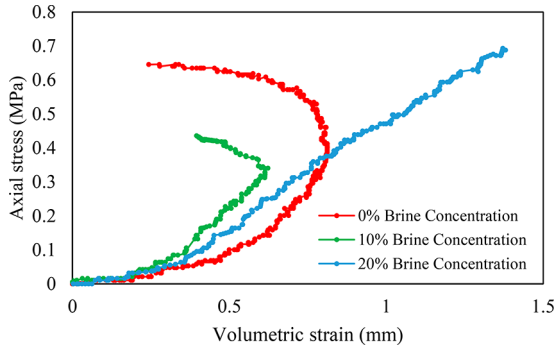

Figure 13. Variation of the volumetric strain with axial stress of coal samples, subjected to uniaxial loading.

Interestingly, the AE response corresponding to the 10% NaCl saturation is quite similar to that at 0% concentration, showing a very low cumulative AE count as well as a considerable crack closure time, which infers no significant fracture propagation took place during the loading (see Figure 10b). In contrast, the fracture density at 10% condition is considerably high (2.11%), compared to water saturation. The possible reason for high fracture density at 10% NaCl concentration is that, unlike in water saturation, there should be coal mass-brine reactions occurred during the saturation: (1) forming new micro cracks by interconnecting existing cracks and (2) widening/extending the existing parent cracks through chemical corrosions at the fracture−matrix interface areas and at crack tips (which also contributed to strength reduction). The fracture aperture distribution covers a wide range (i.e., 0.032−0.446 mm) (see Table 4), concluding that much thinner micro cracks (~0.032 mm) occurred in the coal mass and the existing natural cracks were widened due to the corrosive chemical interaction. The enhanced stress corrosion and material dissolution at fracture surfaces under acidic environment can cause these new crack formations and strength

DOI: 10.1021/acs.energyfuels.8b00577
Energy Fuels 2018, 32, 5799−5811

reduction. Formation of thinner micro cracks and the expansion of parent cracks, contribute to the increment of overall fracture density of the sample (i.e., ≈70% increment compared to water saturation). As explained by Li et al.,[61] the initial crack length, fracture toughness, and the fracture density are the crucial parameters that affect the deformation behavior of a rock mass. Congruent with this explanation, the ARAMIS image map shows the highest strain distribution (see Figure 12b), and the sample exhibits a dilatancy behavior upon loading (see Figure 13), all of which confirm the softer nature and the higher plastic deformation undergone by the samples due to the existence of excessive fractures in the samples saturated at 10% brine concentration.

Figure 10c shows the AE count for 20% NaCl concentration with a very low crack closure time, which suggests that the fracture initiation started soon after the load application. The large AE count of 1960 and long stable and unstable crack propagation period implies that the fracture propagation occurred almost continuously throughout the loading period. The fracture quantification from the micro-CT image data agrees with this observation as it can be clearly seen from the ortho-slice that the induced fracture network is very dense (2.65%) but thinner (average fracture aperture of 0.151 mm) (see Figure 11c and Table 4). The possible reason for the thinner fracture network should be the crystal accumulation at pores near the sample surface during the air drying, which induced a brittleness in to the sample. In fact, the sample brittleness index has been increased by 19.6%, when compared with the water saturation condition (see Table 3). The higher brittleness (77.13%) has precluded the plastic deformation of the sample, obviating the fracture widening upon mechanical loading. Moreover, the reason for high AE count and high fracture density should be due to the occurrence of brittle fractures and crystal crushing, upon mechanical loading. The ARAMIS image analysis confirms this observation, as the strain contour map shows no significant strain variation at the sample failure, where the samples failed before undergoing an extensive plastic deformation (see Figure 12c). The volumetric strain variation as illustrated in Figure 13 shows no dilatancy behavior but only a compaction during the complete loading period, until failure. This implies that the corrosive interaction of the coal-brine and resultant coal softening have been overcome by the excessive brine accumulation, so that the ensemble sample acts mechanistically as brittle rock. Thus, the results reveal that the very high brine concentration has produced a significant crystal accumulation in the near-surface pores during surface drying, imparting a brittle response and an elevated strength to the sample, resulting in the propagation of a dense and thinner fracture network during loading.

Overall, the interpretation of strength and brittleness variation, deformation pattern, fracture propagation, and induced fracture characteristics give a clear indication of how the different brine concentrations in the pore fluid alter the coal mass mechanical behavior. It should be noted that the changes in the fracture network can occur in two stages, viz. during the saturation period and during the external load application. During the saturation, the natural fracture network in the coal mass can be severely altered due to (1) coal softening effect during water saturation and (2) corrosive chemical interactions due to ionic concentration in the saturation fluid. The fracture propagation and induced fracture characteristics during the load application under experimental conditions also vary with brine concentration due to varying brittleness. However, the interpretation of results from sensitive analyses such as AE analysis should be completed carefully, to avoid being misdirected with false results due to the salinity of the pore fluid. The AE counts due to pore fluid saturation with high brine concentrations may indicate a more brittle failure or more cracking in the rock mass. However, this could also be happened due to the crushing of precipitated NaCl crystals in the near-surface pores.

The conclusions yielded from this study give a clear insight on how the coal mass mechanical properties vary with different brine saturation concentrations and how the fracture characteristics vary during brine saturation and mechanical loading. Enhanced coal seam gas extraction in industry is incorporated with several reservoir stimulation methods such as hydraulic fracturing. The efficiency of such methods depends on the induced fracture density and the fracture aperture, as they control the enhanced rock permeability and ultimate gas production. Also, a safer stimulation method always depends on the reservoir mechanical properties, such as strength, brittleness, and stiffness. The knowledge given by the study is important in coal seam gas recovery, as it comprehensively discusses the mechanical behavior and evolution of fracture characteristics, both of which are important for implementing effective and safer gas extraction methods. The results suggest that rocks under water and brine saturated conditions can create a wider fracture network due to fracture initiating/reopening and high plastic deformation. However, this may cause irreversible damage to the coal mass during the external load applications due to lower strength and lower stiffness of the rock. The extensive fracture network created in this manner could also contaminate adjacent aquifers through the leakage of methane and fracture fluids. Thus, the stimulation methods like hydraulic fracturing should carefully be designed by addressing the pore fluid characteristics as well as the pumping schedule, since it can severely alter the mechanical properties of rock mass, especially in sensitive rocks like coal.

CONCLUSIONS

Among various factors, brine concentration of the pore fluid is an important parameter that may control the efficiency of hydraulic fracturing. Different NaCl concentrations in pore fluids can cause irreversible alterations in coal pore structure and in the resulting induced fracture networks. The following conclusions are drawn from a comprehensive study exploring the mechanical, microstructural, chemical, and acoustic emission characterization of coal samples permeated with different brine concentrations (i.e., 0%, 10%, and 20% NaCl by weight) and failed under uniaxial loading.

(1) EDS and XRD analyses of both natural and saturated coal specimens provide no evidence of significant additional minerals or chemical constituents other than native carbon and oxygen found on the brown coal samples used in the study. Thus, all the variations in results are as a result of the interaction between coal mass and applied brines.

(2) Compared to natural coal strength, a strength reduction may occur at water saturation, as water molecules easily react with the mineral and clay content of the rock specimen and soften the bond structure. With increasing brine concentrations (order of 10%), the available ionic concentration triggers chemical interactions between the pore fluid and the coal mass, resulting in a significant reduced strength.

(3) At higher order of NaCl concentrations like 20%, which are closer to the solubility limit of NaCl in water, the crystal

DOI: 10.1021/acs.energyfuels.8b00577
Energy Fuels 2018, 32, 5799−5811

accumulation in near-surface pores during air drying may dominate over the reaction based strength reduction, imparting a high strength and a brittleness to the sample. However, the so-called crystal accumulations or strength regains cannot be anticipated in reservoir conditions, because the NaCl in CSG water remains dissolved due to a higher degree of saturation and low ionic concentration.

(4) The AE analysis and the qualitative and quantitative analysis of the resulting fracture networks at varying brine concentrations infer that fracture characteristics of a brine saturated coal mass, subjected to uniaxial loading, can be varied due to a number of reasons: (1) fracture reopening due to coal softening during saturation, (2) micro crack initiation and extension/widening of natural cracks due to corrosive chemical interactions between coal mass and ions in saturation fluid, and (3) expansion of existing cracks and initiation of new cracks during mechanical loading.

(5) The strain contour maps and the volumetric deformation analyses show that the brine saturated coal specimens subjected to mechanical loading exhibit a dilatancy behavior, confirming the higher plastic deformation undergone by the samples because of the softer nature and the volume expansion due to existence of excessive fractures in the samples.

The results of the study reveals that mechanical properties and the induced fracture characteristics of coal masses can be greatly impacted by the native pore fluid characteristics. It should be noted that although the fracture network become dense and wide during brine saturation, the resulting coal mass is weak and soft, so that the mechanically induced fractures may be extensive with the danger that the rock formation is damaged and that adjacent aquifers may be contaminated by fugitive fluids. Therefore, stimulation methods such as hydraulic fracturing should be implemented with care in such sensitive reservoirs, in order to beneficially enhance gas extraction but to minimize potential reservoir damage.

AUTHOR INFORMATION

Corresponding Author

*Phone: +61 3 9035 8649. E-mail: samintha.perera@unimelb.edu.au.

ORCID

M. S. A. Perera: 0000-0002-6784-0544

P. G. Ranjith: 0000-0003-0094-7141

Notes

The authors declare no competing financial interest.

REFERENCES

(1) International Energy Agency (IEA). *Key world energy statistics*,https://www.iea.org/publications/freepublications/publication/KeyWorld2017.pdf, 2017.

(2) Perera, M. S. A.; Ranjith, P. G.; Choi, S. K.; Bouazza, A.; Kodikara, J.; Airey, D. A review of coal properties pertinent to carbon dioxide sequestration in coal seams: with special reference to Victorian brown coals. *Environ. Earth Sci.* **2011**, *64* (1), 223−235.

(3) Durie, R. A. *The Science of Victorian Brown Coal: Structure, Properties and Consequences from Utilization*; Butterworth, Heinemann: Oxford, 1991.

(4) Buccino, S.; Steve, J. Controlling water pollution from coalbed methane drilling: An analysis of discharge permit requirements. *Wyo. L. Rev.* **2004**, *4*, 559−584.

(5) Sampath, K. H. S. M.; Perera, M. S. A.; Ranjith, P. G.; Matthai, S. K.; Rathnaweera, T.; Zhang, G.; Tao, X. CH_4-CO_2 gas exchange and supercritical CO_2 based hydraulic fracturing as CBM production-accelerating techniques: A review. *Journal of CO_2 Utilization* **2017**, *22*, 212−230.

(6) Bartos, T. T.; Ogle, K. M. *Water quality and environmental isotopic analyses of ground-water samples collected from the Wasatch and Fort Union formations in areas of coalbed methane development: implications to recharge and ground-water flow, eastern Powder River Basin, Wyoming*, Water-Resources Investigations Report 02-4045, U.S. Department of the Interior, U.S. Geological Survey: Cheyenne, WY, 2002.

(7) McBeth, I. H.; Reddy, K. J.; Skinner, Q. D. Coalbed methane product water chemistry in three Wyoming watersheds. *J. Am. Water Resour. Assoc.* **2003**, *39* (3), 575−585.

(8) Patz, M. J.; Ready, K. J.; Skinner, Q. D. Chemistry of coalbed methane discharge water interacting with semi-arid ephemeral stream channels. *J. Am. Water Resour. Assoc.* **2004**, *40* (5), 1247−1255.

(9) Jackson, R. E.; Reddy, K. J. Geochemistry of coalbed natural gas (CBNG) produced water in Powder River Basin, Wyoming: salinity and sodicity. *Water, Air, Soil Pollut.* **2007**, *184* (1−4), 49−61.

(10) Kinnon, E. C. P.; Golding, S. D.; Boreham, C. J.; Baublys, K. A.; Esterle, J. S. Stable isotope and water quality analysis of coal bed methane production waters and gases from the Bowen Basin, Australia. *Int. J. Coal Geol.* **2010**, *82* (3), 219−231.

(11) Decker, A. D.; Klusman, R.; Horner, D. M. Geochemical techniques applied to the identification and disposal of connate coal water. In *Coalbed Methane Symposium*, Tuscaloosa, Alabama, 1987; pp 229−242.

(12) Van Voast, W. A. Geochemical signature of formation waters associated with coalbed methane. *AAPG Bull.* **2003**, *87* (4), 667−676.

(13) Taulis, M.; Milke, M. Chemical variability of groundwater samples collected from a coal seam gas exploration well, Maramarua, New Zealand. *Water Res.* **2013**, *47* (3), 1021−1034.

(14) Ranjith, P. G.; Perera, M. S. A.; Khan, E. A study of safe CO2 storage capacity in saline aquifers: a numerical study. *Int. J. Energy Res.* **2013**, *37* (3), 189−199.

(15) Rathnaweera, T. D.; Ranjith, P. G.; Perera, M. S. A. Salinity-dependent strength and stress−strain characteristics of reservoir rocks in deep saline aquifers: An experimental study. *Fuel* **2014**, *122*, 1−11.

(16) Shukla, R.; Ranjith, P. G.; Choi, S. K.; Haque, A.; Yellishetty, M.; Hong, L. Mechanical behaviour of reservoir rock under brine saturation. *Rock mechanics and rock engineering* **2013**, *46* (1), 83−93.

(17) Feucht, L. J.; Logan, J. M. Effects of chemically active solutions on shear behaviour of a sandstone. *Tectonophysics* **1990**, *175*, 159−176.

(18) Rathnaweera, T. D.; Ranjith, P. G.; Perera, M. S. A.; Haque, A.; Lashin, A.; Al Arifi, N.; Chandrasekharam, D.; Yang, S. Q.; Xu, T.; Wang, S. H.; Yasar, E. CO2-induced mechanical behaviour of Hawkesbury sandstone in the Gosford basin: An experimental study. *Mater. Sci. Eng., A* **2015**, *641*, 123−137.

(19) Fox, A.; Snelling, P.; McKenna, J.; Neale, C.; Neuhaus, C.; Miskimins, J. Geomechanical Principles for Unconventional Reservoirs. *Microseismic* **2013**.

(20) Zhang, D.; Ranjith, P. G.; Perera, M. S. A. The brittleness indices used in rock mechanics and their application in shale hydraulic fracturing: A review. *J. Pet. Sci. Eng.* **2016**, *143*, 158−170.

(21) Alassi, H. T.; Holt, R. M.; Nes, O.-m.; Pradhan, S. Realistic geomechanical modeling of hydraulic fracturing in fractured reservoir rock. In *Canadian Unconventional Resources Conference*, Society of Petroleum Engineers, 2011.

(22) Slatt, R. M.; Abousleiman, Y. Multiscale, Brittle-Ductile Couplets in Unconventional Gas Shales: Merging Sequence Stratigraphy and Geomechanics. In *AAPG Annual Convention and Exhibition*, Houston, TX, 2011; pp 10−13.

(23) Jin, X.; Shah, S. N.; Roegiers, J.-C.; Zhang, B. Fracability evaluation in shale reservoirs-an integrated petrophysics and geomechanics approach. *SPE Hydraulic Fracturing Technology Conference* **The Woodlands, Texas, USA 2014**, *Society of Petroleum Engineers*, 518−526.

(24) Minerals Council of Australia−Victorian Division. *Minerals fact sheets- Brown coal- Lignite*, http://www.minerals.org.au/file_upload/files/resources/victoria/minerals_fact_sheets/Minerals_-_Fact_Sheets_-_Brown_Coal_-_Lignite.pdf.

DOI: 10.1021/acs.energyfuels.8b00577
Energy Fuels 2018, 32, 5799−5811

(25) Sakaguchi, M.; Laursen, K.; Nakagawa, H.; Miura, K. Hydrothermal upgrading of Loy Yang Brown coal—Effect of upgrading conditions on the characteristics of the products. *Fuel Process. Technol.* **2008**, *89* (4), 391−396.
(26) Sydney Catchment Authority. *Coal Seam Gas impacts on water resources*, 2012.
(27) ASTM. *D. 2938, Standard Test Method for Unconfined Compressive Strength of Intact Rock Core Specimens*, ASTM International: West Conshohocken, PA.
(28) Grigore, M.; Sakurovs, R. Inorganic matter in Victorian brown coals. *Int. J. Coal Geol.* **2016**, *154*, 257−264.
(29) Ruan, C.-D.; Ward, C. R. Quantitative X-ray powder diffraction analysis of clay minerals in Australian coals using Rietveld methods. *Appl. Clay Sci.* **2002**, *21* (5), 227−240.
(30) Murakami, K.; Ozaki, J.-i.; Nishiyama, Y. Effects of surface treatment on cation exchange properties of Australian brown coals. *Fuel Process. Technol.* **1995**, *43* (1), 95−110.
(31) Lafferty, C.; Hobday, M. The use of low rank brown coal as an ion exchange material: 1. Basic parameters and the ion exchange mechanism. *Fuel* **1990**, *69* (1), 78−83.
(32) Domazetis, G.; James, B. D. Molecular models of brown coal containing inorganic species. *Org. Geochem.* **2006**, *37*, 244−259.
(33) Fuerstenau, D. W.; Rosenbaum, J. M.; You, Y. S. Electrokinetic behavior of coal. *Energy Fuels* **1988**, *2* (3), 241−245.
(34) Langmuir, D. *Aqueous Environmental Geochemistry*; Prentice Hall, 1997..
(35) Labus, K.; Bujok, P. CO_2 mineral sequestration mechanisms and capacity of saline aquifers of the Upper Silesian Coal Basin (Central Europe)-Modeling and experimental verification. *Energy* **2011**, *36* (8), 4974−4982.
(36) Holdren, G. R.; Berner, R. A. Mechanism of feldspar weathering - 1. Experimental studies. *Geochim. Cosmochim. Acta* **1979**, *43* (8), 1161−1171.
(37) Marbler, H.; Erickson, K. P.; Schmidt, M.; Lempp, C.; Pöllmann, H. Geomechanical and geochemical effects on sandstones caused by the reaction with supercritical CO_2: an experimental approach to in situ conditions in deep geological reservoirs. *Environ. Earth Sci.* **2013**, *69* (6), 1981−1998.
(38) Hucka, V.; Das, B. Brittleness determination of rocks by different methods. *International Journal of Rock Mechanics and Mining Sciences & Geomechanics Abstracts* **1974**, *11* (10), 389−392.
(39) Viete, D. R.; Ranjith, P. G. The effect of CO_2 on the geomechanical and permeability behaviour of brown coal: Implications for coal seam CO_2 sequestration. *Int. J. Coal Geol.* **2006**, *66*, 204−216.
(40) Perera, M. S. A.; Ranjith, P. G.; Peter, M. Effects of saturation medium and pressure on strength parameters of Latrobe Valley brown coal: Carbon dioxide, water and nitrogen saturations. *Energy* **2011**, *36*, 6941−6947.
(41) Brady, B. H.; Brown, E. T. *Rock Mechanics: For Underground Mining*; Springer Science & Business Media, 2013.
(42) Van Eeckhout, E. M. The mechanisms of strength reduction due to moisture in coal mine shales. *International Journal of Rock Mechanics and Mining Sciences & Geomechanics Abstracts* **1976**, *13* (2), 61−67.
(43) Lama, R. D.; Vutukuri, V. S., *Handbook on Mechanical Properties of Rocks-Testing Techniques and Results*; Trans Tech Publications: Bay Village, OH, 1978; Vol. 2.
(44) Zhang, Y.; Lebedev, M.; Sarmadivaleh, M.; Barifcani, A.; Rahman, T.; Iglauer, S. Swelling effect on coal micro structure and associated permeability reduction. *Fuel* **2016**, *182*, 568−576.
(45) Zhang, Y.; Lebedev, M.; Al-Yaseri, A.; Yu, H.; Xu, X.; Sarmadivaleh, M.; Barifcani, A.; Iglauer, S. Nanoscale rock mechanical property changes in heterogeneous coal after water adsorption. *Fuel* **2018**, *218*, 23−32.
(46) Johns, R. B.; Chaffee, A. L.; Harvey, K. F.; Buchanan, A. S.; Thiele, G. A. The conversion of brown coal to a dense, dry, hard material. *Fuel Process. Technol.* **1989**, *21* (3), 209−221.
(47) Dunning, J. D.; Miller, M. E. Effects of pore fluid chemistry on stable sliding of Berea sandstone. *Pure Appl. Geophys.* **1985**, *122* (2), 447−462.
(48) Swolfs, H. S. *Influence of pore-fluid chemistry and temperature on fracture of sandstone under confining pressure*. Texas A&M University, College Station, TX, 1971.
(49) Fryer, J. F.; Szladow, A. J. *Storage of Coal Samples*; ARC/AGS Information Series, Vol. *66*; Alberta Research Council, 1973.
(50) Eberhardt, E.; Stead, D.; Stimpson, B. Quantifying progressive pre-peak brittle fracture damage in rock during uniaxial compression. *International journal of rock mechanics and mining sciences & geomechanics* **1999**, *36* (3), 361−380.
(51) Ranjith, P. G.; Fourar, M.; Pong, S. F.; Chian, W.; Haque, A. Characterisation of fractured rocks under uniaxial loading states. *International journal of rock mechanics and mining sciences & geomechanics* **2004**, *41*, 43−48.
(52) Pickerd, V. *Optimisation and Validation of the ARAMIS Digital Image Correlation System for Use in Large-Scale High-Strain-Rate Events*, No. DSTO-TN-1203. Defense Science and Technology Organization Victoria (Australia) Maritime Division, 2013.
(53) Lyu, Q.; Ranjith, P. G.; Long, X.; Kang, Y.; Huang, M. Effects of coring directions on the mechanical properties of Chinese shale. *Arabian J. Geosci.* **2015**, *8* (12), 10289−10299.
(54) Lyu, Q.; Long, X.; Ranjith, P. G.; Kang, Y. Unconventional gas: Experimental study of the influence of subcritical carbon dioxide on the mechanical properties of black shale. *Energies* **2016**, *9* (7), 516−530.
(55) Ranathunga, A. S.; Perera, M. S. A.; Ranjith, P. G.; Bui, H. Super-critical CO2 saturation-induced mechanical property alterations in low rank coal: An experimental study. *J. Supercrit. Fluids* **2016**, *109*, 134−140.
(56) Carlson, W. D.; Rowe, T.; Ketcham, R. A.; Colbert, M. W. *Applications of High-Resolution X-ray Computed Tomography in Petrology, Meteoritics and Palaeontology*; Geological Society: London, 2003; Special Publications, Vol. *215*, (1), 7−22.
(57) Zhang, Y.; Xu, X.; Lebedev, M.; Sarmadivaleh, M.; Barifcani, A.; Iglauer, S. Multi-scale x-ray computed tomography analysis of coal microstructure and permeability changes as a function of effective stress. *Int. J. Coal Geol.* **2016**, *165*, 149−156.
(58) Zhang, Y.; Sarmadivaleh, M.; Barifcani, A.; Lebedev, M.; Iglauer, S. Coal microstructure changes due to water absorption and CO_2 injection. *APPEA J.* **2016**, *56* (2), 593−593.
(59) Ramandi, H. L.; Mostaghimi, P.; Armstrong, R. T.; Saadatfar, M.; Pinczewski, W. V. Porosity and permeability characterization of coal: a micro-computed tomography study. *Int. J. Coal Geol.* **2016**, *154*, 57−68.
(60) Ramandi, H. L.; Armstrong, R. T.; Mostaghimi, P. Micro-CT image calibration to improve fracture aperture measurement. *Case Studies in Nondestructive Testing and Evaluation* **2016**, *6*, 4−13.
(61) Li, C.; Prikryl, R.; Nordlund, E. The stress-strain behaviour of rock material related to fracture under compression. *Eng. Geol.* **1998**, *49* (3−4), 293−302.

DOI: 10.1021/acs.energyfuels.8b00577
Energy Fuels 2018, 32, 5799−5811